NANO LETTERS

pubs.acs.org/NanoLett

Letter

# Lattice Reconstruction in $MoSe_2$–$WSe_2$ Heterobilayers Synthesized by Chemical Vapor Deposition

Zhijie Li,[○] Farsane Tabataba-Vakili,*[,○] Shen Zhao,[○] Anna Rupp, Ismail Bilgin, Ziria Herdegen, Benjamin März, Kenji Watanabe, Takashi Taniguchi, Gabriel Ravanhani Schleder, Anvar S. Baimuratov, Efthimios Kaxiras, Knut Müller-Caspary, and Alexander Högele*

Cite This: *Nano Lett.* 2023, 23, 4160–4166

Read Online

ACCESS | Metrics & More | Article Recommendations | Supporting Information

**ABSTRACT:** Vertical van der Waals heterostructures of semiconducting transition metal dichalcogenides realize moiré systems with rich correlated electron phases and moiré exciton phenomena. For material combinations with small lattice mismatch and twist angles as in $MoSe_2$–$WSe_2$, however, lattice reconstruction eliminates the canonical moiré pattern and instead gives rise to arrays of periodically reconstructed nanoscale domains and mesoscopically extended areas of one atomic registry. Here, we elucidate the role of atomic reconstruction in $MoSe_2$–$WSe_2$ heterostructures synthesized by chemical vapor deposition. With complementary imaging down to the atomic scale, simulations, and optical spectroscopy methods, we identify the coexistence of moiré-type cores and extended moiré-free regions in heterostacks with parallel and antiparallel alignment. Our work highlights the potential of chemical vapor deposition for applications requiring laterally extended heterosystems of one atomic registry or exciton-confining heterostack arrays.

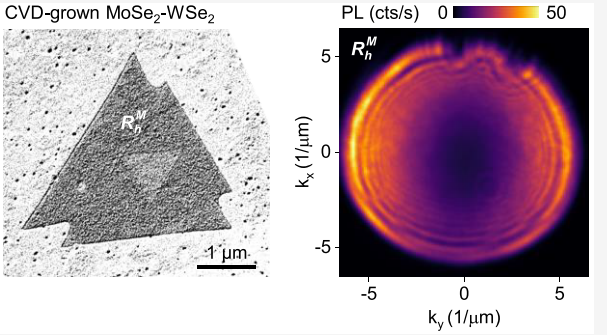


**KEYWORDS:** *two-dimensional semiconductors, $MoSe_2$–$WSe_2$, heterostructures, chemical vapor deposition, lattice reconstruction, atomic registries, interlayer excitons*



Vertical heterostructures of transition metal dichalcogenide semiconductors manifest in two contrasting regimes. On the one hand, exfoliation-stacked heterobilayers with finite lattice mismatch or twist angle give rise to periodic two-dimensional (2D) moiré patterns, which in turn result in flat moiré minibands of charge carriers with rich phenomena of correlated Hubbard model physics.[1−6] Moiré potentials also profoundly affect strongly bound electron–hole pairs in the form of intralayer[7,8] and interlayer[9−12] excitons formed by Coulomb correlations within or across individual layers. This scenario is contrasted by moiré-free heterobilayers on the other hand, obtained from chemical vapor deposition (CVD) synthesis,[13−15] where the absence of lateral moiré potentials is signified by one atomic registry extending laterally over large sample areas[15] with simple photoluminescence (PL) spectra[13] or enhanced diffusion of interlayer excitons.[14] Heterostructure systems with diffusive interlayer excitons represent an ideal material platform for integrated dipolar exciton circuits,[16] as demonstrated recently in exfoliation-stacked heterostructures with an additional interfacial layer of hexagonal boron nitride (hBN), which mitigates the exciton-confining moiré potential.[17,18] Even more promising are CVD-synthesized heterobilayers free of moiré effects, featuring enhanced diffusivity of dipolar interlayer excitons,[14] unaffected by diffusion-inhibiting moiré confinement.[14,19,20] Such moiré-free heterostructures are not only ideal for integrated exciton circuits with external control by electrostatic gates,[21,22] they could also enable deterministically imprinting arbitrary, tunable potential landscapes via patterned gate-electrodes,[23,24] or dielectric superlattices.[25]

Moiré-free domains on micrometer length scales also emerge in heterostructures with small lattice mismatch and marginal twist subject to mesoscopic lattice reconstruction, where the driving mechanism behind atom rearrangement into energetically favorable registries is provided by the competition between intralayer strain and interlayer adhesion energy,[26−28] yielding mesoscopic 2D domains of only one registry in $MoSe_2$–$WSe_2$ stamping-assembled heterostacks.[29] For practical applications, however, such nondeterministic fabrication methods with resulting spatial inhomogeneities in morphology

**Received:** December 29, 2022
**Revised:** March 7, 2023
**Published:** May 4, 2023

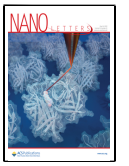





https://doi.org/10.1021/acs.nanolett.2c05094
*Nano Lett.* 2023, 23, 4160–4166

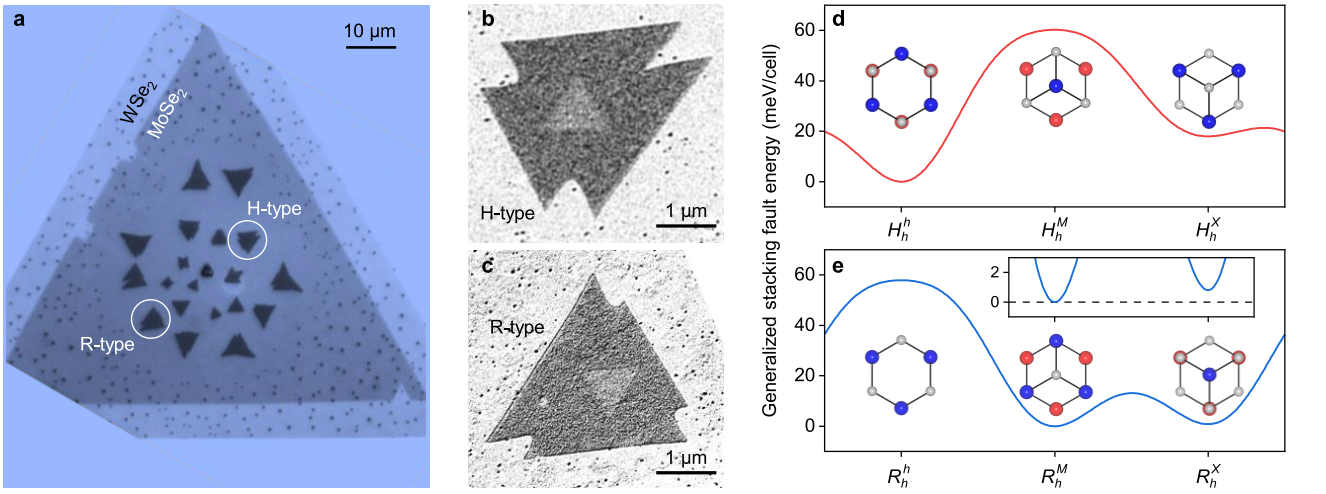


**Figure 1.** $MoSe_2$−$WSe_2$ heterobilayers: sample structure of CVD-synthesized H- and R-type stacks and theory of stacking fault energy. (a) Optical micrograph of an as-grown heterobilayer consisting of a large triangular $MoSe_2$ monolayer with an outer edge of monolayer $WSe_2$ and triangles of monolayer $WSe_2$ on top with 0° (R-type) and 180° (H-type) twist. The white circles indicate the H- and R-type flakes studied by optical spectroscopy. (b, c) SEM images (recorded with secondary electron imaging and shown with inverted black-and-white contrast) of two representative H- and R-type heterobilayers synthesized in the same growth. (d, e) DFT calculations of the generalized stacking fault energy for the different stackings in H- and R-type heterostructures, respectively, including top views of the three high-symmetry atomic registries with W (blue, top layer), Mo (red, bottom layer), and Se (gray) atoms. Inset in part e: Zoom to the minima at $R_h^M$ and $R_h^X$ stackings.

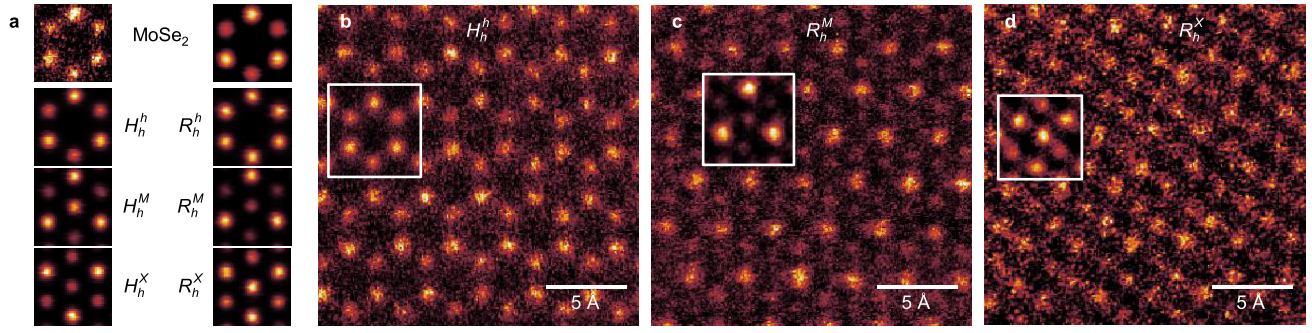


**Figure 2.** HAADF-STEM imaging and simulations. (a) Top row: Measurement (left) and simulation (right) of $MoSe_2$ monolayer. Bottom rows: Simulations of the three high-symmetry stackings in H-type (left column) and R-type (right column) heterostacks. (b−d) HAADF-STEM images of heterobilayers in $H_h^h$, $R_h^M$, and $R_h^X$ stacking, respectively. Insets show images averaged over ten unit cells.

and optical properties[29] limit the required uniformity and scalability, rendering CVD-based approaches to large-area moiré-free systems a promising alternative.

In this work, we present an elaborate study of CVD-synthesized vertical $MoSe_2$−$WSe_2$ heterobilayers with evidence for extended reconstruction into domains of one atomic registry, enclosing a central region of periodically reconstructed nanoscale domains.[26,27,29] Our studies cover both high-symmetry stacking configurations with 0° (R-type) and 180° (H-type) twist angle, and employ complementary imaging and optical spectroscopy methods to identify the diversity in local configurations of the reconstructed crystal lattice and the respective signatures of exciton transitions. Our work highlights the potential of CVD synthesis for obtaining both extended moiré-free domains and exciton-confining arrays of periodically reconstructed moiré regions, realizing the limits of dipolar excitons with and without a spatially varying potential landscape.

Our samples with $MoSe_2$−$WSe_2$ heterobilayers consist of large monolayers of $MoSe_2$ with monolayers of $WSe_2$ on top, both synthesized by CVD in a two-step growth (see Sections 1 and 2 in the Supporting Information for details). Figure 1a depicts an optical micrograph of an as-grown heterobilayer, showing the formation of both H- and R-type stackings. We examined another heterobilayer sample synthesized in the same growth run by scanning electron microscopy (SEM), with representative images shown in Figure 1b,c. The images of H- and R-type samples were recorded with secondary electron imaging with material- and stacking-sensitive contrast[29−31] (see Section 3 in the Supporting Information for details), clearly discerning a small triangle in the center of the heterostack.

Three high-symmetry atomic registries are distinguished in H- and R-type heterostructures, namely $H_h^h$, $H_h^M$, $H_h^X$ and $R_h^h$, $R_h^M$, $R_h^X$, with $M$, $X$, and $h$ referring to the transition metal, chalcogen, and center of the hexagon, and the superscript and subscript to the $MoSe_2$ and $WSe_2$ layer, respectively (note that the nomenclature is chosen to be consistent with previous work[29,32,33]). In Figure 1d,e, we show density functional theory (DFT) calculations of the generalized stacking fault energy (GSFE)[26] for the different atomic registries with local extrema at the three high-symmetry stackings (see Section 4 in the Supporting Information for details) indicated by the respective top-view schematics. Minima in GSFE correspond to the



https://doi.org/10.1021/acs.nanolett.2c05094
Nano Lett. 2023, 23, 4160−4166

energetically most favorable stackings that dominate the reconstruction.[28] In the H-type case shown in Figure 1d, the $H_h^h$ atomic registry is by far the energetically most favorable, consistent with prior work.[26,28,29] In contrast, in the R-type case (Figure 1e) both $R_h^M$ and $R_h^X$ stackings are close to the optimal energy, with $R_h^M$ being slightly more favorable (inset of Figure 1e). This implies close competition between the two registries, with a higher likelihood of $R_h^M$ to form extended domains.

Our study of individual heteroflakes with aberration-corrected high-resolution high-angle annular dark-field scanning transmission electron microscopy (HAADF-STEM) (see Section 5 in the Supporting Information for details) confirms the exclusive dominance of the $H_h^h$ atomic registry in H-type heterostacks, as well as the reconstruction of R-type stacks into $R_h^M$ and $R_h^X$ registries. To begin with, we establish the orientation of the crystallographic axes in the heterobilayers using the surrounding $MoSe_2$ monolayer, with measurement (left) and simulation (right) of the hexagonal lattice shown in the top row of Figure 2a. For this orientation, the bottom rows in Figure 2a show simulations of the three possible high-symmetry stackings in H- and R-type, which compete for energy minimization in reconstruction. In stacks of H-type, our experiments with results as in Figure 2b identify the $H_h^h$ stacking only, in agreement with the theoretical prediction above. In R-type heterostacks, on the other hand, we observe extended areas of $R_h^M$ registry in some flakes (as in Figure 2c), while other flakes exhibit extended areas of $R_h^X$ stacking (as in Figure 2d). Given the close similarity of the two registry configurations with regard to optimal energy, it is plausible that some R-type flakes reconstruct into $R_h^M$ while others take on the $R_h^X$ stacking and that their distribution is stochastic on the flake-to-flake case.

To study the optical properties of CVD-synthesized H- and R-type crystals, we encapsulated the sample shown in Figure 1a in hBN (see Section 6 in the Supporting Information for details) and performed cryogenic confocal PL and differential reflectance (DR) spectroscopy. Each atomic registry uniquely determines the combination of transition energies,[29,32,34] optical selection rules,[32,34,35] and oscillator strengths[36,37] of interlayer excitons and thus provides means for spectroscopic characterization. For our sample, the maps of maximum interlayer exciton PL intensity in H- and R-type heterostructures are shown in Figure 3a,b with dashed lines indicating the heterostack boundaries. The H-type sample shows extended areas of bright interlayer exciton PL (as on the spot marked by the brown cross in Figure 3a) and a dark region near the center (blue cross in Figure 3a). The R-type sample features similar local variations in the PL map, yet with nearly 2 orders of magnitude lower intensity.

The low intensity of R-type as compared to H-type stacks is surprising, as reconstructed mechanically stacked samples support the opposite trend.[29] This observation suggests that domains of $R_h^M$ registry with relatively dark interlayer excitons dominate CVD-grown R-type heterostacks. In the areas of maximum PL intensity marked by brown crosses in Figure 3, a and b, both H- and R-stacks feature simple spectra with dominant peaks at 1.40 and 1.45 eV in Figure 3, c and d, respectively. In the H-stack, the PL peak at 1.40 eV with a positive degree of circular polarization $P_c$ (shown in the bottom panel of Figure 3c) corresponds to the triplet interlayer exciton transition in extended $H_h^h$ domains of reconstructed mechanically stacked samples,[29] and is accompanied by a weak

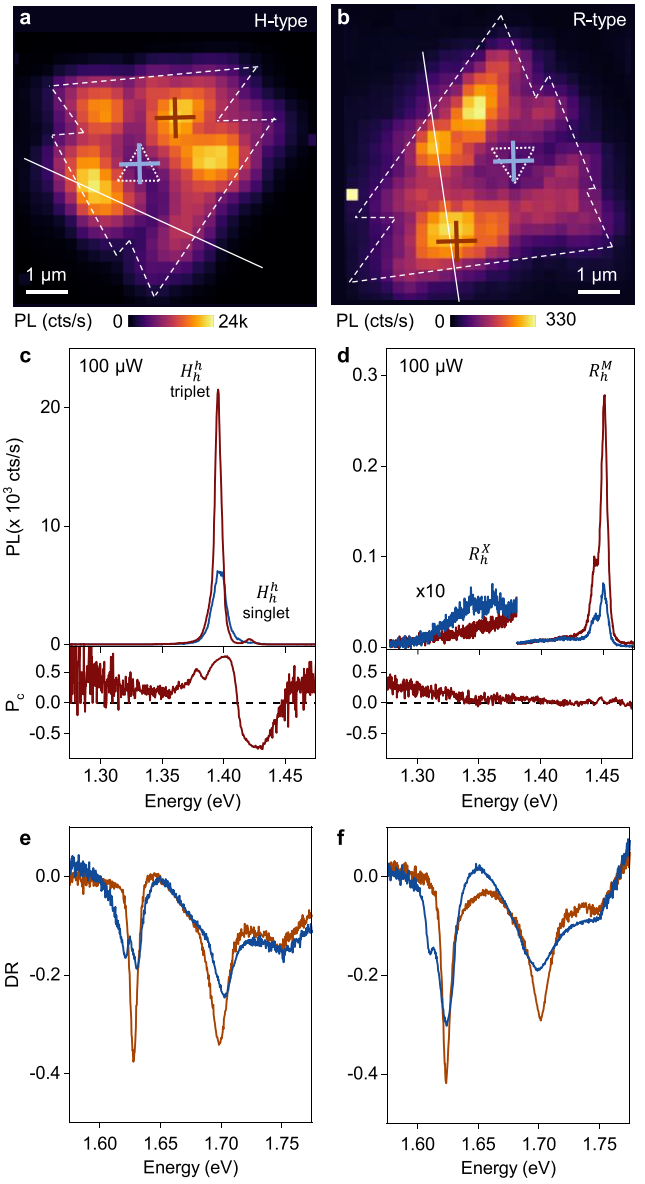


**Figure 3.** CVD-heterobilayers in cryogenic spectroscopy. (a, b) Maps of interlayer PL maximum intensity (dashed lines show flake boundaries from optical images, dotted lines delimit the central triangles, and solid lines indicate from top left to bottom right intensity profiles in Figure 5c,d). (c, d) Top panel: Interlayer exciton PL spectra recorded with linearly polarized excitation and circularly polarized detection at positions shown by the brown and blue crosses in parts a and b (the spectra below 1.37 eV in part d are multiplied by 10 for better visibility), with atomic registries assigned to the corresponding transitions. Bottom panel: Degree of circular polarization $P_c$ measured at the position of the brown cross in parts a and b. (e, f) Differential reflectance (DR) spectra corresponding to areas indicated by brown and blue crosses in parts a and b. All data were recorded at 4 K, with 100 $\mu$W excitation in PL spectroscopy.

hot-luminescence singlet at 1.42 eV with negative $P_c$.[13,29,38,39] The main peak in the R-type stack, on the other hand, is blue-shifted by 120 meV from its counterpart observed on reconstructed $R_h^X$ domains of mechanically stacked heterostructures at 1.33 eV[29] and exhibits zero $P_c$ in Figure 3d. This finding, combined with the PL energy position and reduced relative brightness, corroborates our assumption about the $R_h^M$ character of interlayer exciton states with $z$-polarized


https://doi.org/10.1021/acs.nanolett.2c05094
Nano Lett. 2023, 23, 4160−4166

transitions.[29,35,37] Finally, we observe that areas of maximum PL intensity exhibit simple resonances of intralayer exciton in the DR spectra of H- and R-type stacks (shown in Figure 3e,f for positions indicated by brown crosses in Figure 3a,b) as a hallmark of extended areas of one dominant atomic registry.[29] We also point out the absence of trion-related resonances in the DR spectra of both stacks as a signature of low residual doping, which we also confirmed with PL spectroscopy away from heterostacks on monolayer $MoSe_2$ (data not shown).

In the central areas of H- and R-type stacks marked by blue crosses in the areas of dotted triangles in Figure 3a,b and spectra in Figure 3c,d, we observe reduced intensity of the main PL peaks and an additional spectral feature around 1.35 eV with negative $P_c$ (not shown) in the R-type case. The latter is a feature of $R_h^X$ atomic registry,[29] which coexists with $R_h^M$ in the core of the heterostack. This conclusion, substantiated by the observation of doublets in the DR spectra of Figure 3e,f near the intralayer exciton resonance of $MoSe_2$ at 1.62 eV, identifies the central triangles as arrays of reconstructed quasi zero-dimensional (0D) domains,[29] which can form as nanoscale hexagons of $H_h^h$ registry in H-type and in triangular tiling of $R_h^X$ and $R_h^M$ domains in R-type stacks.[28] Although the spatial resolution of the SEM in secondary-electron imaging is insufficient to detect the actual tiling geometry, the difference in the contrast between the outer regions of both types of heterostacks and their triangular cores in Figure 1b,c provides compelling support for the assignment of the triangular centers to reconstructed 0D arrays.

To elaborate on the nature of interlayer excitons in extended $R_h^M$ domains not reported previously for $MoSe_2$−$WSe_2$ heterostacks, we performed angle-resolved PL measurements. Using momentum-space imaging[40] with the 2D $k$-space profile shown in Figure 4a for the PL from a bright H-type area, we first confirm the in-plane character of the optical dipole orientation for $H_h^h$ interlayer excitons for reference. Their Gaussian emission profile, with highest intensity at zero in-plane $k$-vector in the linecut at $k_x = 0$ (bottom panel of Figure 4a) is contrasted by the R-type case in Figure 4b: The PL emission in the energy range 1.43−1.46 eV assigned to $R_h^M$ atomic registry is nearly zero at small $k$-vectors and increases with increasing $k$ as a hallmark of out-of-plane dipole moment orientation.[41] With the detection angle of 54° of our objective, we observe the PL from out-of-plane oriented interlayer excitons in $R_h^M$ atomic registry, which are dark at normal incidence and exhibit $z$-polarized emission according to dipolar selection rules.[35]

To complete the correspondence between the signatures of interlayer excitons in stamping-assembled[29] and CVD-synthesized heterostacks studied here, we discuss the results of magneto-luminescence experiments in Faraday configuration shown in Figure 4c,d for H- and R-type stacks, respectively. In finite magnetic fields, the interlayer triplet and singlet excitons in domains of $H_h^h$ atomic registry feature circularly polarized transitions, with linear valley Zeeman splitting given by $\Delta_z = E^+ - E^- = g\mu_B B$ (with magnetic field $B$, Bohr magneton $\mu_B$, exciton Landé factor $g$, and $E^\pm$ referring to the dispersion branch measured under $\sigma^+$ and $\sigma^-$ detection). The triplet and singlet transitions differ characteristically in both sign and magnitude of their exciton Landé $g$-factors, determined from the slopes of simultaneous linear fits to the data in Figure 4c as $-17.0 \pm 0.4$ and $+11.5 \pm 0.3$, respectively, in agreement with DFT calculations[29,33,37] and previous experiments.[9,29,39,42−45] In the R-type case, the magnetic field dependence of the $z$-polarized $R_h^M$ interlayer exciton is given by $E^\pm = E_0 \pm \frac{1}{2}\sqrt{\delta^2 + \Delta_z^2}$ with zero-field exciton energy without exchange interaction $E_0$ and exchange splitting $\delta$.[46] In Figure 4d, both dispersion branches are observed in both circular polarizations, and respecting the sign convention we thus obtain from the fit to the data with $\delta = 0.1$ meV the absolute value of the exciton Landé factor as $|g| = 6.5$. The $g$-factor is in quantitative agreement with DFT, predicting a value of 6.3.[29,37] In the central triangle (data not shown), we determine for $R_h^X$ an interlayer exciton $g$-factor of $+7.0 \pm 0.2$ in agreement with previous experiments and theory.[9,29,33,39]

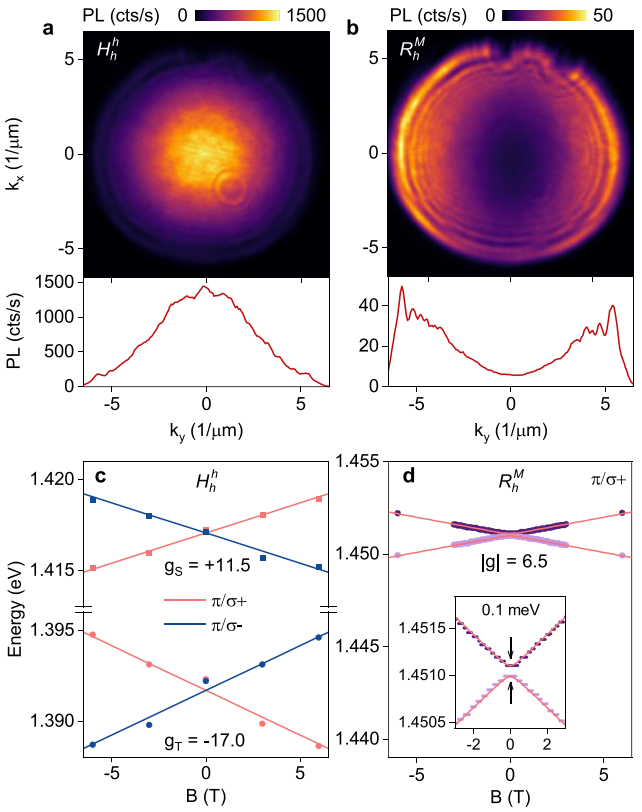


**Figure 4.** Momentum-space and magneto-optical characteristics of interlayer exciton luminescence. (a, b) Top panels: Momentum-space maps of interlayer exciton PL in H- and R-type samples, respectively (tunable long- and short-pass filters were used to limit the detection in part b to the energy range of 1.43−1.46 eV). Bottom panels: Emission profiles at $k_x = 0$. (c, d) Magneto-dispersion recorded under linearly polarized excitation and circularly polarized detection, with Landé $g$-factors extracted from fits to the data. Inset in part d: Zoom to the dispersion around zero field, with emphasis on the dark exciton exchange splitting $\delta$ of 0.1 meV. All measurements were performed at 100 $\mu$W excitation power and 4 K.

Last, we note that in between extended bright areas in the PL maps of Figure 3a,b, we observed reduced PL intensities, which we ascribe to grain boundaries separating reconstructed 2D domains. Figure 5a shows PL and $P_c$ spectra at such a dark position in the H-type stack with $H_h^h$ triplet and singlet exciton characteristics and slightly reduced $P_c$ as compared to a bright spot with data in Figure 3c. The variations in the PL intensity of $H_h^h$ interlayer excitons in Figure 5c is consistent with local reduction in emission (dip around 4 $\mu$m with width given by the optical spot) in between two bright areas separated by a grain boundary. At the corresponding positions with reduced PL in the R-type stack, we observe additional contributions


https://doi.org/10.1021/acs.nanolett.2c05094
Nano Lett. 2023, 23, 4160−4166

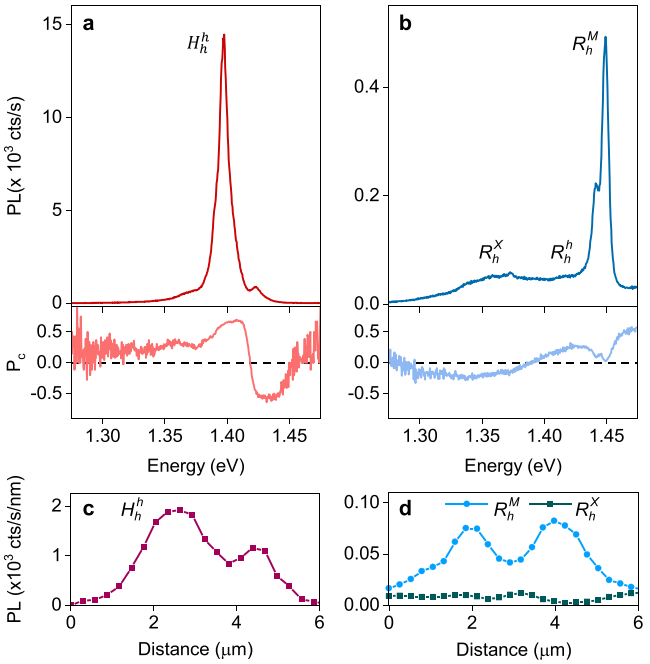


**Figure 5.** Spectral characteristics of grain boundaries. (a, b) Top and bottom panels: Interlayer exciton PL spectra and degree of circular polarization $P_c$ at grain boundaries in H- and R-type samples, respectively. (c, d) Spatial variations in the interlayer exciton PL of different atomic registries upon lateral transition from one bright spot to another indicated in the maps of Figure 3. All measurements were performed at 100 $\mu$W excitation power and 4 K.

from $R_h^X$ and $R_h^h$ atomic registries with spectra in Figure 5b and negative and positive $P_c$, respectively.[29,35] The spatial intensity profiles of $R_h^M$ and $R_h^X$ interlayer exciton PL in Figure 5d are anticorrelated, identifying grain boundaries as mutually exclusive areas of competing registries with additional contribution from $R_h^h$ interlayer excitons via hot luminescence.[29]

The comparison of spectral characteristics of CVD-grown $MoSe_2$–$WSe_2$ heterostacks with our prior work on mechanically stacked samples[29] yields qualitatively equivalent results anticipated from general theoretical considerations. In H-type stacks, we found domains of $H_h^h$ atomic registry to dominate extended areas of heterostacks, encompassing a triangular core of 0D domains. In R-type stacks, $R_h^M$ and $R_h^X$ domains coexist in triangular cores of CVD-heteroflakes and compete for mutually exclusive reconstruction in the surrounding domains. In R-type stacks with extended domains of $R_h^M$ atomic registries, we identify the spectral signatures of interlayer excitons not reported previously from mechanically stacked samples. We anticipate that in CVD-grown heterostacks reconstruction takes place during high-temperature synthesis and thus is robust against postprocessing steps of sample transfer or annealing at much lower temperatures. With extended reconstructed 2D domains and 0D arrays in their inner cores, CVD-grown $MoSe_2$–$WSe_2$ heterostacks realize areas of both moiré-free and moiré-like systems. While the latter are technologically viable as quantum dot arrays of exciton-confining potentials on the nanoscale[32,34] and the former for dipolar exciton circuitry and extrinsic gate-modulation of potential landscapes,[16,21,22] grain boundaries between domains of different atomic registries could host excitons with topological protection.[47]

## ■ ASSOCIATED CONTENT

### Supporting Information

The Supporting Information is available free of charge at https://pubs.acs.org/doi/10.1021/acs.nanolett.2c05094.

Synthesis of $MoSe_2$–$WSe_2$ heterobilayers, sample fabrication, SEM imaging, theoretical modeling, STEM imaging, and optical spectroscopy (PDF)

## ■ AUTHOR INFORMATION


### Corresponding Authors

**Farsane Tabataba-Vakili** − *Fakultät für Physik, Munich Quantum Center, and Center for NanoScience (CeNS), Ludwig-Maximilians-Universität München, 80539 München, Germany; Munich Center for Quantum Science and Technology (MCQST), 80799 München, Germany;* orcid.org/0000-0001-5911-7594; Email: f.tabataba@lmu.de

**Alexander Högele** − *Fakultät für Physik, Munich Quantum Center, and Center for NanoScience (CeNS), Ludwig-Maximilians-Universität München, 80539 München, Germany; Munich Center for Quantum Science and Technology (MCQST), 80799 München, Germany;* orcid.org/0000-0002-0178-9117; Email: alexander.hoegele@lmu.de

### Authors

**Zhijie Li** − *Fakultät für Physik, Munich Quantum Center, and Center for NanoScience (CeNS), Ludwig-Maximilians-Universität München, 80539 München, Germany*

**Shen Zhao** − *Fakultät für Physik, Munich Quantum Center, and Center for NanoScience (CeNS), Ludwig-Maximilians-Universität München, 80539 München, Germany*

**Anna Rupp** − *Fakultät für Physik, Munich Quantum Center, and Center for NanoScience (CeNS), Ludwig-Maximilians-Universität München, 80539 München, Germany*

**Ismail Bilgin** − *Fakultät für Physik, Munich Quantum Center, and Center for NanoScience (CeNS), Ludwig-Maximilians-Universität München, 80539 München, Germany*

**Ziria Herdegen** − *Department of Chemistry and Center for NanoScience, Ludwig-Maximilians-Universität München, 81377 München, Germany*

**Benjamin März** − *Department of Chemistry and Center for NanoScience, Ludwig-Maximilians-Universität München, 81377 München, Germany;* orcid.org/0000-0003-1628-9868

**Kenji Watanabe** − *Research Center for Functional Materials, National Institute for Materials Science, Tsukuba 305-0044, Japan;* orcid.org/0000-0003-3701-8119

**Takashi Taniguchi** − *International Center for Materials Nanoarchitectonics, National Institute for Materials Science, Tsukuba 305-0044, Japan;* orcid.org/0000-0002-1467-3105

**Gabriel Ravanhani Schleder** − *John A. Paulson School of Engineering and Applied Sciences, Harvard University, Cambridge, Massachusetts 02138, United States*

**Anvar S. Baimuratov** − *Fakultät für Physik, Munich Quantum Center, and Center for NanoScience (CeNS), Ludwig-Maximilians-Universität München, 80539 München, Germany*

**Efthimios Kaxiras** − *John A. Paulson School of Engineering and Applied Sciences, Harvard University, Cambridge, Massachusetts 02138, United States; Department of Physics,*




https://doi.org/10.1021/acs.nanolett.2c05094
Nano Lett. 2023, 23, 4160−4166

*Harvard University, Cambridge, Massachusetts 02138, United States*

**Knut Müller-Caspary** − *Department of Chemistry and Center for NanoScience, Ludwig-Maximilians-Universität München, 81377 München, Germany*

Complete contact information is available at: https://pubs.acs.org/10.1021/acs.nanolett.2c05094

### Author Contributions

○Z. L., F. T.-V. and S. Z. contributed equally to this work.

### Notes

The authors declare no competing financial interest.

## ■ ACKNOWLEDGMENTS

This research was funded by the European Research Council (ERC) under Grant Agreement No. 772195 as well as the Deutsche Forschungsgemeinschaft (DFG, German Research Foundation) within the Priority Programme SPP 2244 2DMP and Germany's Excellence Strategy under Grant No. EXC-2111-390814868 and EXC-2089-390776260. Z.L. was supported by the China Scholarship Council (CSC), grant No. 201808140196. F.T.-V. acknowledges funding from the Munich Center for Quantum Science and Technology and the European Union's Framework Programme for Research and Innovation Horizon Europe under the Marie Skłodowska-Curie Actions Grant Agreement No. 101058981. S.Z. and I.B. acknowledge funding from the Alexander von Humboldt Foundation, and A.S.B. acknowledges funding from the European Union's Framework Programme for Research and Innovation Horizon 2020 (2014−2020) under the Marie Skłodowska-Curie Grant Agreement No. 754388 (LMUR-esearchFellows) and from LMUexcellent, funded by the Federal Ministry of Education and Research (BMBF) and the Free State of Bavaria under the Excellence Strategy of the German Federal Government and the Länder. A.R., K.M.-C. and A.H. acknowledge funding by the Bavarian Hightech Agenda within the Munich Quantum Valley doctoral fellowship program and the EQAP project. G.R.S. acknowledges funding from the Army Research Office under Cooperative Agreement No. W911NF-21-2-0147. E.K. acknowledges funding from the STC Center for Integrated Quantum Materials, NSF Grant No. DMR-1231319, NSF DMREF Award No. 1922172, and the Army Research Office under Cooperative Agreement No. W911NF-21-2-0147. K.W. and T.T. acknowledge support from JSPS KAKENHI (grant No. 19H05790, 20H00354 and 21H05233).

## ■ REFERENCES

(1) Wu, F.; Lovorn, T.; Tutuc, E.; MacDonald, A. H. Hubbard model physics in transition metal dichalcogenide moiré bands. *Phys. Rev. Lett.* **2018**, *121*, 026402.

(2) Tang, Y.; Li, L.; Li, T.; Xu, Y.; Liu, S.; Barmak, K.; Watanabe, K.; Taniguchi, T.; MacDonald, A. H.; Shan, J.; Mak, K. F. Simulation of Hubbard model physics in $WSe_2/WS_2$ moiré superlattices. *Nature* **2020**, *579*, 353.

(3) Shimazaki, Y.; Schwartz, I.; Watanabe, K.; Taniguchi, T.; Kroner, M.; Imamoğlu, A. Strongly correlated electrons and hybrid excitons in a moiré heterostructure. *Nature* **2020**, *580*, 472.

(4) Regan, E. C.; Wang, D.; Jin, C.; Bakti Utama, M. I.; Gao, B.; Wei, X.; Zhao, S.; Zhao, W.; Zhang, Z.; Yumigeta, K.; Blei, M.; Carlström, J. D.; Watanabe, K.; Taniguchi, T.; Tongay, S.; Crommie, M.; Zettl, A.; Wang, F. Mott and generalized Wigner crystal states in $WSe_2/WS_2$ moiré superlattices. *Nature* **2020**, *579*, 359.

(5) Xu, Y.; Liu, S.; Rhodes, D. A.; Watanabe, K.; Taniguchi, T.; Hone, J.; Elser, V.; Mak, K. F.; Shan, J. Correlated insulating states at fractional fillings of moiré superlattices. *Nature* **2020**, *587*, 214.

(6) Tang, Y.; Gu, J.; Liu, S.; Watanabe, K.; Taniguchi, T.; Hone, J. C.; Mak, K. F.; Shan, J. Dielectric catastrophe at the Mott and Wigner transitions in a moiré superlattice. *Nat. Commun.* **2022**, *13*, 4271.

(7) Zhang, N.; Surrente, A.; Baranowski, M.; Maude, D. K.; Gant, P.; Castellanos-Gomez, A.; Plochocka, P. Moiré intralayer excitons in a $MoSe_2/MoS_2$ heterostructure. *Nano Lett.* **2018**, *18*, 7651.

(8) Naik, M. H.; Regan, E. C.; Zhang, Z.; Chan, Y.-H.; Li, Z.; Wang, D.; Yoon, Y.; Ong, C. S.; Zhao, W.; Zhao, S.; Utama, M. I. B.; Gao, B.; Wei, X.; Sayyad, M.; Yumigeta, K.; Watanabe, K.; Taniguchi, T.; Tongay, S.; da Jornada, F. H.; Wang, F.; Louie, S. G. Intralayer charge-transfer moiré excitons in van der Waals superlattices. *Nature* **2022**, *609*, 52.

(9) Seyler, K. L.; Rivera, P.; Yu, H.; Wilson, N. P.; Ray, E. L.; Mandrus, D. G.; Yan, J.; Yao, W.; Xu, X. Signatures of moiré-trapped valley excitons in $MoSe_2/WSe_2$ heterobilayers. *Nature* **2019**, *567*, 66.

(10) Tran, K.; Moody, G.; Wu, F.; Lu, X.; Choi, J.; Kim, K.; Rai, A.; Sanchez, D. A.; Quan, J.; Singh, A.; Embley, J.; Zepeda, A.; Campbell, M.; Autry, T.; Taniguchi, T.; Watanabe, K.; Lu, N.; Banerjee, S. K.; Silverman, K. L.; Kim, S.; Tutuc, E.; Yang, L.; MacDonald, A. H.; Li, X. Evidence for moiré excitons in van der Waals heterostructures. *Nature* **2019**, *567*, 71.

(11) Jin, C.; Regan, E. C.; Yan, A.; Iqbal Bakti Utama, M.; Wang, D.; Zhao, S.; Qin, Y.; Yang, S.; Zheng, Z.; Shi, S.; Watanabe, K.; Taniguchi, T.; Tongay, S.; Zettl, A.; Wang, F. Observation of moiré excitons in $WSe_2/WS_2$ heterostructure superlattices. *Nature* **2019**, *567*, 76.

(12) Alexeev, E. M.; Ruiz-Tijerina, D. A.; Danovich, M.; Hamer, M. J.; Terry, D. J.; Nayak, P. K.; Ahn, S.; Pak, S.; Lee, J.; Sohn, J. I.; Molas, M. R.; Koperski, M.; Watanabe, K.; Taniguchi, T.; Novoselov, K. S.; Gorbachev, R. V.; Shin, H. S.; Fal'ko, V. I.; Tartakovskii, A. I. Resonantly hybridized excitons in moiré superlattices in van der Waals heterostructures. *Nature* **2019**, *567*, 81.

(13) Hsu, W.-T.; Lu, L.-S.; Wu, P.-H.; Lee, M.-H.; Chen, P.-J.; Wu, P.-Y.; Chou, Y.-C.; Jeng, H.-T.; Li, L.-J.; Chu, M.-W.; Chang, W.-H. Negative circular polarization emissions from $WSe_2/MoSe_2$ commensurate heterobilayers. *Nat. Commun.* **2018**, *9*, 1356.

(14) Choi, J.; Hsu, W.-T.; Lu, L.-S.; Sun, L.; Cheng, H.-Y.; Lee, M.-H.; Quan, J.; Tran, K.; Wang, C.-Y.; Staab, M.; Jones, K.; Taniguchi, T.; Watanabe, K.; Chu, M.-W.; Gwo, S.; Kim, S.; Shih, C.-K.; Li, X.; Chang, W.-H. Moiré potential impedes interlayer exciton diffusion in van der Waals heterostructures. *Sci. Adv.* **2020**, *6*, No. eaba8866.

(15) Xia, J.; Yan, J.; Wang, Z.; He, Y.; Gong, Y.; Chen, W.; Sum, T. C.; Liu, Z.; Ajayan, P. M.; Shen, Z. Strong coupling and pressure engineering in $WSe_2$-$MoSe_2$ heterobilayers. *Nat. Phys.* **2021**, *17*, 92.

(16) Butov, L. V. *Excitonic devices, Superlattices and Microstructures* **2017**, *108*, 2.

(17) Sun, Z.; Ciarrocchi, A.; Tagarelli, F.; Gonzalez Marin, J. F.; Watanabe, K.; Taniguchi, T.; Kis, A. Excitonic transport driven by repulsive dipolar interaction in a van der Waals heterostructure. *Nat. Photonics* **2022**, *16*, 79.

(18) Shanks, D. N.; Mahdikhanysarvejahany, F.; Stanfill, T. G.; Koehler, M. R.; Mandrus, D. G.; Taniguchi, T.; Watanabe, K.; LeRoy, B. J.; Schaibley, J. R. Interlayer exciton diode and transistor. *Nano Lett.* **2022**, *22*, 6599.

(19) Yuan, L.; Zheng, B.; Kunstmann, J.; Brumme, T.; Kuc, A. B.; Ma, C.; Deng, S.; Blach, D.; Pan, A.; Huang, L. Twist-angle-dependent interlayer exciton diffusion in $WS_2$-$WSe_2$ heterobilayers. *Nat. Mater.* **2020**, *19*, 617.

(20) Wang, J.; Shi, Q.; Shih, E.-M.; Zhou, L.; Wu, W.; Bai, Y.; Rhodes, D.; Barmak, K.; Hone, J.; Dean, C. R.; Zhu, X.-Y. Diffusivity Reveals Three Distinct Phases of Interlayer Excitons in $MoSe_2/WSe_2$ Heterobilayers. *Phys. Rev. Lett.* **2021**, *126*, 106804.

(21) Jiang, Y.; Chen, S.; Zheng, W.; Zheng, B.; Pan, A. Interlayer exciton formation, relaxation, and transport in TMD van der Waals heterostructures. *Light Sci. Appl.* **2021**, *10*, 72.

(22) Ciarrocchi, A.; Tagarelli, F.; Avsar, A.; Kis, A. Excitonic devices with van der Waals heterostructures: valleytronics meets twistronics. *Nat. Rev. Mater.* **2022**, *7*, 449.
(23) Shanks, D. N.; Mahdikhanysarvejahany, F.; Muccianti, C.; Alfrey, A.; Koehler, M. R.; Mandrus, D. G.; Taniguchi, T.; Watanabe, K.; Yu, H.; LeRoy, B. J.; Schaibley, J. R. Nanoscale trapping of interlayer excitons in a 2D semiconductor heterostructure. *Nano Lett.* **2021**, *21*, 5641.
(24) Shanks, D. N.; Mahdikhanysarvejahany, F.; Koehler, M. R.; Mandrus, D. G.; Taniguchi, T.; Watanabe, K.; LeRoy, B. J.; Schaibley, J. R. Single exciton trapping in an electrostatically defined 2D semiconductor quantum dot. *Phys. Rev. B* **2022**, *106*, L201401.
(25) Shi, L.-k.; Ma, J.; Song, J. C. Gate-tunable flat bands in van der Waals patterned dielectric superlattices. *2D Mater.* **2020**, *7*, 015028.
(26) Carr, S.; Massatt, D.; Torrisi, S. B.; Cazeaux, P.; Luskin, M.; Kaxiras, E. Relaxation and domain formation in incommensurate two-dimensional heterostructures. *Phys. Rev. B* **2018**, *98*, 224102.
(27) Enaldiev, V.; Zólyomi, V.; Yelgel, C.; Magorrian, S.; Fal'ko, V. Stacking domains and dislocation networks in marginally twisted bilayers of transition metal dichalcogenides. *Phys. Rev. Lett.* **2020**, *124*, 206101.
(28) Rosenberger, M. R.; Chuang, H.-J.; Phillips, M.; Oleshko, V. P.; McCreary, K. M.; Sivaram, S. V.; Hellberg, C. S.; Jonker, B. T. Twist angle-dependent atomic reconstruction and moiré patterns in transition metal dichalcogenide heterostructures. *ACS Nano* **2020**, *14*, 4550.
(29) Zhao, S.; Li, Z.; Huang, X.; Rupp, A.; Göser, J., Vovk, I. A.; Kruchinin, S. Y.; Watanabe, K.; Taniguchi, T.; Bilgin, I.; Baimuratov, A. S.; Högele, A. Excitons in mesoscopically reconstructed moiré heterostructures. *arXiv preprint* 2022; arXiv:2202.11139;https://arxiv.org/abs/2202.11139 (accessed March 3, 2022).
(30) Ashida, K.; Kajino, T.; Kutsuma, Y.; Ohtani, N.; Kaneko, T. Crystallographic orientation dependence of SEM contrast revealed by SiC polytypes. *J. Vac. Sci. Technol. B* **2015**, *33*, 04E104.
(31) Andersen, T. I.; Scuri, G.; Sushko, A.; De Greve, K.; Sung, J.; Zhou, Y.; Wild, D. S.; Gelly, R. J.; Heo, H.; Bérubé, D.; Joe, A. Y.; Jauregui, L. A.; Watanabe, K.; Taniguchi, T.; Kim, P.; Park, H.; Lukin, M. D. Excitons in a reconstructed moiré potential in twisted $WSe_2$/$WSe_2$ homobilayers. *Nat. Mater.* **2021**, *20*, 480.
(32) Yu, H.; Liu, G.-B.; Tang, J.; Xu, X.; Yao, W. Moiré excitons: From programmable quantum emitter arrays to spin-orbit−coupled artificial lattices. *Sci. Adv.* **2017**, *3*, No. e1701696.
(33) Woźniak, T.; Faria Junior, P. E.; Seifert, G.; Chaves, A.; Kunstmann, J. Exciton g-factors of van der Waals heterostructures from first principles calculations. *Phys. Rev. B* **2020**, *101*, 235408.
(34) Wu, F.; Lovorn, T.; MacDonald, A. Theory of optical absorption by interlayer excitons in transition metal dichalcogenide heterobilayers. *Phys. Rev. B* **2018**, *97*, 035306.
(35) Förg, M.; Colombier, L.; Patel, R. K.; Lindlau, J.; Mohite, A. D.; Yamaguchi, H.; Glazov, M. M.; Hunger, D.; Högele, A. Cavity-control of interlayer excitons in van der Waals heterostructures. *Nat. Commun.* **2019**, *10*, 3697.
(36) Gillen, R.; Maultzsch, J. Interlayer excitons in $MoSe_2$/$WSe_2$ heterostructures from first principles. *Phys. Rev. B* **2018**, *97*, 165306.
(37) Förg, M.; Baimuratov, A. S.; Kruchinin, S. Y.; Vovk, I. A.; Scherzer, J.; Förste, J.; Funk, V.; Watanabe, K.; Taniguchi, T.; Högele, A. Moiré excitons in $MoSe_2$-$WSe_2$ heterobilayers and heterotrilayers. *Nat. Commun.* **2021**, *12*, 1656.
(38) Hanbicki, A. T.; Chuang, H.-J.; Rosenberger, M. R.; Hellberg, C. S.; Sivaram, S. V.; McCreary, K. M.; Mazin, I. I.; Jonker, B. T. Double indirect interlayer exciton in a $MoSe_2$/$WSe_2$ van der Waals heterostructure. *ACS Nano* **2018**, *12*, 4719.
(39) Joe, A. Y.; Jauregui, L. A.; Pistunova, K.; Mier Valdivia, A. M.; Lu, Z.; Wild, D. S.; Scuri, G.; De Greve, K.; Gelly, R. J.; Zhou, Y.; Sung, J.; Sushko, A.; Taniguchi, T.; Watanabe, K.; Smirnov, D.; Lukin, M. D.; Park, H.; Kim, P. Electrically controlled emission from singlet and triplet exciton species in atomically thin light-emitting diodes. *Phys. Rev. B* **2021**, *103*, L161411.
(40) Dominguez, D.; Alharbi, N.; Alhusain, M.; Bernussi, A. A.; Peralta, L. G. d. Fourier plane imaging microscopy. *J. Appl. Phys.* **2014**, *116*, 103102.
(41) Li, Z.; Wang, T.; Lu, Z.; Khatoniar, M.; Lian, Z.; Meng, Y.; Blei, M.; Taniguchi, T.; Watanabe, K.; McGill, S. A.; Tongay, S.; Menon, V. M.; Smirnov, D.; Shi, S.-F. Direct observation of gate-tunable dark trions in monolayer $WSe_2$. *Nano Lett.* **2019**, *19*, 6886.
(42) Nagler, P.; Ballottin, M. V.; Mitioglu, A. A.; Mooshammer, F.; Paradiso, N.; Strunk, C.; Huber, R.; Chernikov, A.; Christianen, P. C. M.; Schüller, C.; Korn, T. Giant magnetic splitting inducing near-unity valley polarization in van der Waals heterostructures. *Nat. Commun.* **2017**, *8*, 1551.
(43) Wang, T.; Miao, S.; Li, Z.; Meng, Y.; Lu, Z.; Lian, Z.; Blei, M.; Taniguchi, T.; Watanabe, K.; Tongay, S.; Smirnov, D.; Shi, S.-F. Giant Valley-Zeeman Splitting from Spin-Singlet and Spin-Triplet Interlayer Excitons in $WSe_2$/$MoSe_2$ Heterostructure. *Nano Lett.* **2020**, *20*, 694.
(44) Delhomme, A.; Vaclavkova, D.; Slobodeniuk, A.; Orlita, M.; Potemski, M.; Basko, D. M.; Watanabe, K.; Taniguchi, T.; Mauro, D.; Barreteau, C.; Giannini, E.; Morpurgo, A. F.; Ubrig, N.; Faugeras, C. Flipping exciton angular momentum with chiral phonons in $MoSe_2$/$WSe_2$ heterobilayers. *2D Mater.* **2020**, *7*, 041002.
(45) Brotons-Gisbert, M.; Baek, H.; Molina-Sánchez, A.; Campbell, A.; Scerri, E.; White, D.; Watanabe, K.; Taniguchi, T.; Bonato, C.; Gerardot, B. D. Spin−layer locking of interlayer excitons trapped in moiré potentials. *Nat. Mater.* **2020**, *19*, 630.
(46) Robert, C.; Amand, T.; Cadiz, F.; Lagarde, D.; Courtade, E.; Manca, M.; Taniguchi, T.; Watanabe, K.; Urbaszek, B.; Marie, X. Fine structure and lifetime of dark excitons in transition metal dichalcogenide monolayers. *Phys. Rev. B* **2017**, *96*, 155423.
(47) Chaves, A.; Covaci, L.; Peeters, F. M.; Milošević, M. V. Topologically protected moiré exciton at a twist-boundary in a van der Waals heterostructure. *2D Mater.* **2022**, *9*, 025012.


https://doi.org/10.1021/acs.nanolett.2c05094
*Nano Lett.* 2023, 23, 4160−4166